

**Document Version**

Final published version

**Licence**

CC BY

**Citation (APA)**

Abdelrahman, M., Yang, C., Khaloian, A., Achterhold, K., Pfeiffer, F., & Van De Kuilen, J. W. (2026). Influence of frequency and recovery interval on fatigue behavior of wood in compression. *Holzforschung*, *80*(2), 99-114. <https://doi.org/10.1515/hf-2025-0104>

**Important note**

To cite this publication, please use the final published version (if applicable). Please check the document version above.

**Copyright**

In case the licence states "Dutch Copyright Act (Article 25fa)", this publication was made available Green Open Access via the TU Delft Institutional Repository pursuant to Dutch Copyright Act (Article 25fa, the Taverne amendment). This provision does not affect copyright ownership.

Unless copyright is transferred by contract or statute, it remains with the copyright holder.

**Sharing and reuse**

Other than for strictly personal use, it is not permitted to download, forward or distribute the text or part of it, without the consent of the author(s) and/or copyright holder(s), unless the work is under an open content license such as Creative Commons.

**Takedown policy**

Please contact us and provide details if you believe this document breaches copyrights. We will remove access to the work immediately and investigate your claim.

## Wood Physics/Mechanical Properties

Mostafa Abdelrahman\*, Changxi Yang, Ani Khaloian, Klaus Achterhold, Franz Pfeiffer and Jan-Willem van de Kuilen

# Influence of frequency and recovery interval on fatigue behavior of wood in compression

<https://doi.org/10.1515/hf-2025-0104>

Received September 8, 2025; accepted November 14, 2025;  
published online December 29, 2025

**Abstract:** This study investigates the fatigue behavior of European ash (*Fraxinus excelsior*) with density range of 580–620 kg/m<sup>3</sup> under relatively short-period cyclic compressive loading. The aim is to understand its mechanical behavior, such as: strain development, recovery, and internal damage mechanisms. Mechanical testings at varying frequencies (0.1, 1.0, and 10 Hz) were performed and the samples were scanned with micro-computed tomography (Micro-CT). Multi-scale assessment of fatigue effects was performed. Strain behavior revealed progressive increases in both viscous and viscoelastic components, demonstrating time- and rate-dependent deformation. For the same loading time, higher loading frequencies resulted in consistently lower accumulated strain; however, no significant differences in

strain recovery were observed between frequency groups. Strength and stiffness showed minimal change after up to 2,000 loading cycles at 78 % stress level, highlighting relatively high fatigue resistance of wood under compression. Micro-CT imaging detected internal microcracks in samples pre-loaded with fatigue, inferring that cyclic loading induces more microstructural damage than static conditions. These findings enhance the understanding of the fatigue mechanism in European ash and highlight Micro-CT as a valuable non-destructive tool for internal damage assessment under fatigue loading.

**Keywords:** wood fatigue; residual strength; strain recovery; loading frequency; wood compression

## 1 Introduction

For thousands of years, wood has played an important role in human civilization, finding use in different applications from prosthetics to musical instruments, furniture, large-scale structures like bridges, wind towers, and windmills. Over time, these structures experience repeated loadings, which may lead to fatigue stresses and potential structural failure. Therefore, a thorough understanding of wood's fatigue behavior is essential for designing durable and reliable wooden structures. Fatigue research was initiated by early 20th-century, when the demands in transportation infrastructure, particularly for aerospace applications and railway bridges increased (Lewis 1962). In recent decades, the scope has been enlarged in large scale structures such as, wind turbine blade design (Bond and Ansell 1998; Bonfield and Ansell 1991; Tsai and Ansell 1990). Most of these investigations have focused on high-cycle fatigue (HCF) scenarios, in which materials are subjected to a high number of cycles at low stress levels typical of everyday service loads.

Still, low-cycle fatigue (LCF) is relatively understudied despite its engineering relevance. Existing research has primarily emphasized the effects of repeated loading on the cyclic stiffness and residual strength of wood up to failure, but has largely overlooked strain development and

---

Mostafa Abdelrahman and Changxi Yang contributed equally to this work.

**\*Corresponding author: Mostafa Abdelrahman**, Department of Materials Engineering, Technical University of Munich, Winzererstrasse 45, Munich, 80797, Bavaria, Germany; and Department of Civil Engineering, Suez Canal University, 4.5Km the Ring Road, Ismailia, 8366004, Egypt, E-mail: mostafa.abdelrahman@tum.de. <https://orcid.org/0000-0003-2732-5780>

**Changxi Yang and Ani Khaloian**, Department of Materials Engineering, Technical University of Munich, Winzererstrasse 45, Munich, 80797, Bavaria, Germany, E-mail: changxi.yang@tum.de (C. Yang), khaloian@hfm.tum.de (A. Khaloian). <https://orcid.org/0009-0009-2338-9665> (C. Yang)

**Klaus Achterhold**, Department of Physics, TUM School of Natural Sciences and Munich Institute of Biomedical Engineering, Technical University of Munich, 85748 Garching, Germany, E-mail: klaus.achterhold@tum.de

**Franz Pfeiffer**, Department of Physics, TUM School of Natural Sciences and Munich Institute of Biomedical Engineering, Technical University of Munich, 85748 Garching, Germany; and Institute for Diagnostic and Interventional Radiology, School of Medicine and Health, TUM Klinikum, Technical University of Munich, Munich, Germany, E-mail: franz.pfeiffer@tum.de

**Jan-Willem van de Kuilen**, Department of Materials Engineering, Technical University of Munich, Winzererstrasse 45, Munich, 80797, Bavaria, Germany; and Department of Engineering Structures, Delft University of Technology, Stevinweg 1, Delft, 2628, The Netherlands, E-mail: vandekuilen@hfm.tum.de

relaxation after load removal (Clorius 2002; Clorius et al. 2000; Gong and Smith 2000, 2005). This knowledge gap is becoming crucial as timber regains prominence in modern construction, where understanding material performance under different loading conditions is essential for proper design and long-term reliability.

The stress-life (S–N) methodology has served as the primary tool for evaluating wood’s fatigue characteristics, especially for high-cycle fatigue (HCF) analysis. However, it has limitations in capturing material behavior under a low number of load cycles, where the fatigue life cannot be reached. Moreover, irregular loading patterns and complex environmental conditions in practice make the fatigue life evaluation based on S–N approach challenging. These gaps highlight the need for methodological advancements in wood fatigue research.

The fatigue mechanism of wood is influenced by a range of mechanical loading factors, such as stress level (SL) – defined as the ratio of applied stress to ultimate short-term strength – load frequency, load direction, waveform, and load ratio (R). These parameters have been investigated previously by the authors, highlighting their influence on strain development and fatigue life of wood (Yang et al. 2025). For instance, negative R values indicate reversed fatigue loading, which has been shown to be more severe than repetitive loading; the data collected from reversed fatigue tests indicate that failure rarely occurs below 50 % SL within 10 million cycles, regardless of the loading type. Additionally, the frequency of loading can lead to different material responses; very low frequencies, for example, can mimic sustained loading conditions, as demonstrated by Bach (1975).

Although there hasn’t been a systematic investigation into the moisture content influence on fatigue of wood, individual studies have been conducted to compare the fatigue resistance at different relative humidity levels in bending (Lewis 1962; Tsai and Ansell 1990) and compression (Clorius et al. 2000), all suggesting a longer fatigue life at lower relative humidity levels. Furthermore, varying moisture content has been shown to accelerate creep deformation of wood in combination with mechanical loading – the so-called “mechano-sorption” mechanism (Armstrong and Christensen 1961). This could affect the fatigue behavior of wood in a similar way.

The viscoelastic nature of wood further complicates its fatigue behavior. Under sustained stress, wood undergoes creep, and under sustained strain, it exhibits stress relaxation. These phenomena are well-recognized in fatigue studies. Gillwald (1961), for instance, distinguished between recoverable viscoelastic strain and irrecoverable viscous strain. Bach (1973) quantitatively characterized these components using low-cycle compressive fatigue tests, showing

that lower stress levels result in higher relative viscosity but consistent viscoelastic recovery. However, Bach’s methodology, based on matching specimens and assuming identical fatigue lives across grouped samples may not fully account for the natural variability in wood properties.

Understanding the fatigue behavior of wood under parallel-to-grain compression is crucial for the design of structural elements such as columns and their connections. However, bending fatigue has been the most extensively studied loading mode. For this loading configuration, the failure of Japanese cedar and selangan batu is reported to initiate in the compression zone due to the high compressive stresses (Sasaki et al. 2014; Watanabe et al. 2014). This observation underscores the need for a deeper understanding of compressive fatigue mechanisms. The failure mode under compression is strongly influenced by anatomical characteristics such as growth ring orientation, fiber alignment, and microstructural composition. To monitor microstructural damage – such as kink bands, fiber buckling, and cell wall deformation – several techniques, including scanning electron microscopy (SEM) and polarized light microscopy, have been employed (Curtu et al. 1969; Okuyama and Marsoem 1987; Rose 1965; Tsai and Ansell 1990).

This study investigates the effect of loading interval on the behavior of medium-density European ash (*Fraxinus excelsior*) under cyclic compression-compression loading. It focuses on how loading frequency influences short-term strength, stiffness, and strain development and recovery. Three loading frequencies – 0.1 Hz, 1 Hz, and 10 Hz – are tested to evaluate their impact on the mechanical response of the wood. In addition, CT scanning is used to compare internal damage between fatigued and non-fatigued specimens.

## 2 Load direction and frequency

A previous study by the authors (Yang et al. 2025) systematically examined the fatigue behavior of wood under different loading types (uniaxial compression, tension, and bending) for both repeated ( $R \geq 0$ ) and reversed ( $R < 0$ ) loading conditions. Most of the prior research relied on the S–N curve to describe the fatigue mechanism of wood. However, conclusions drawn from S–N curve comparisons cannot be attributed solely to one fatigue parameter. For instance, most bending fatigue studies have been performed under reversed loading. Although bending appears to be a much more severe case when comparing S–N curves from the entire database, it is not significantly different from compression or tension when comparing only repeated cases (Yang et al. 2025).

Compression fatigue of wood has not been extensively studied, despite its relevance in many structural applications. The quasi-static tests of Bach (1973) on pine under  $R = \infty$  conditions demonstrated remarkable fatigue resistance, with specimens enduring over  $10^7$  cycles at 80 % of ultimate stress in parallel-to-grain loading. Similar behavior was observed by Bonfield and Ansell (Bonfield and Ansell 1991) for Douglas fir under  $R = 10$  loading at a 4 Hz frequency, where stress levels of 60–70 % consistently produced lifetimes exceeding  $10^6$  cycles.

Under low-cycle fatigue (LCF) conditions, several studies have attempted to characterize wood performance under compression parallel to the grain. Gong (2002) and Gong and Smith (2005) examined straight-grained spruce at three stress levels (75 %, 85 %, and 95 % of ultimate strength) under triangular waveform loading with a frequency of 0.2 Hz. The authors highlighted that the residual strength of fatigued samples was higher than the reference short-term strength. They also noted a nonlinear influence of stress level on the strain, developed during cyclic loading, which in turn affects material stiffness. Another study by Clorius (2002) investigated the fatigue mechanism of spruce in the parallel-to-grain direction under repeated square wave loading at a stress level of 80 % of ultimate stress and reported a slight increase in short-term strength for fatigued samples compared to those tested only in short-term conditions. A summary of up-to-date literature on low-cycle fatigue of wood and wood products is provided in Table A1 in the Appendix, detailing experimental parameters including species, loading direction, frequency, stress level, number of cycles, waveform, and test conditions.

Frequency effects on fatigue performance exhibit a notable dependence on the uniaxial loading regime. Bach (1975) conducted repeated compression square wave fatigue tests on spruce, exploring frequencies ranging from 0.000001 Hz to 0.1 Hz. His results showed that at the same stress level (SL), specimens could withstand a higher number of cycles to failure as frequency increased. At lower frequencies, the loading acted similarly to a sustained condition, where the duration of load theory applied. Additionally, a study by Clorius et al. (2000) on spruce subjected to repeated cyclic compression fatigue parallel to the grain highlighted a non-linear increase in the number of cycles to failure as loading frequency increased from 0.01 Hz to 10 Hz, accompanied by a reduction in the total time to failure. Clorius et al. (2000) additionally explored the influence of humidity, observing that specimens conditioned at 85 % relative humidity had a longer fatigue life in the 10 Hz group, while those conditioned at 65 % exhibited a reduced fatigue life. The significant influence of frequency on stress-strain

hysteresis and fatigue lifetime was also highlighted in the same study.

For higher frequency levels, Karr et al. (2022) conducted a study on fully reversed tension-compression loading of birch wood, finding that fatigue lifetimes were not significantly affected by testing frequency within the range of 50 Hz to 20 kHz. The strong agreement between the S–N curves at both frequencies, with overlapping standard deviations, suggests that frequency effects are negligible under reversed loading conditions. These results are consistent with a previous study on sycamore maple by Schönbauer et al. (2022), further supporting the negligible impact of frequency on fatigue performance under high-frequency reversed loading conditions.

### 3 Physical changes under fatigue

During fatigue loading, strain develops as a combination of viscoelastic (recoverable) and viscous (irrecoverable) components. Gillwald (1961) demonstrated this in displacement-controlled bending fatigue tests. Regarding compression, the experimental findings by Yang et al. (2025) using European ash under parallel-to-grain compressive fatigue (1 Hz, 78 % SL) reveal increasing strain across loading intervals, with partial recovery during a 10-min recovery period. The residual strain progressively accumulates, confirming the presence of both viscoelastic and viscous strain components.

Cyclic stiffness is a key parameter for evaluating material degradation under fatigue conditions. Various techniques have been developed to monitor changes in stiffness during and after cyclic loading. Gong and Smith (2004); Hacker (1995) defined cyclic stiffness based on the stress-strain range per cycle, calculated as the average slope between the maximum and minimum stress for each loading cycle, as shown in Eq. (1):

$$E_N = \frac{\sigma_{N, \text{Max}} - \sigma_{N, \text{Min}}}{\varepsilon_{N, \text{Max}} - \varepsilon_{N, \text{Min}}} \quad (1)$$

Where,  $\sigma_N^{\text{Max}}$  and  $\sigma_N^{\text{Min}}$  denote the maximum and minimum stress values within each loading cycle, respectively, while  $\varepsilon_N^{\text{Max}}$  and  $\varepsilon_N^{\text{Min}}$  represent the corresponding maximum and minimum strain values. Meanwhile, Clorius et al. (2000) distinguished the stiffness into loading and unloading components by monitoring changes in the slope of the tangents to each cycle on the stress-strain curve. Ogawa et al. (2017); Watanabe et al. (2014) focused solely on the loading phase, evaluating stiffness based on the slope between the stress and strain values corresponding to 30–70 % of the maximum stress for each cycle.

Cyclic stiffness evolution also depends on the type of loading. Reversed loading typically results in a consistent reduction in stiffness. In contrary, tension leads to stepwise reductions likely due to crack propagation, and compression tends to show irregular patterns. Under low-cycle fatigue (LCF) in compression, stiffness changes during cyclic loading are often minimal. Gong (2002) observed no significant change in stiffness at low stress levels (SL) for spruce loaded in compression parallel to the grain, but reported abrupt drops in stiffness near failure under high SL. Similar findings were reported by Ogawa et al. (2017) for Japanese cedar under compression perpendicular to the grain, where stiffness either slightly increased or fluctuated under low SL due to radial densification, but generally decreased under high SL. Yang et al. (2025) further confirmed this trend for European ash tested in compression parallel to the grain, reporting no visible stiffness change during the first 1,000 loading cycles.

The failure mechanism of wood under fatigue loading is highly influenced by its structural formulation. Microscopic techniques such as optical microscopy and scanning electron microscopy (SEM) have been widely used to investigate the initiation and propagation of cracks after cyclic loading. Gong (2002); Gong and Smith (2005) reported that under compressive fatigue, damage in spruce initiated from both pre-existing and cyclically induced kink bands, which were clearly visible using polarized microscopy. The number of kinks correlated well with the deformation and time to failure, concluding that the higher the number of cycles, the more kinks are produced. Okuyama et al. (1984) found no clear distinction in failure modes between different stress levels. In addition, in some cases, specimens with visible buckling lines did not fail even after extended loading. In compression, residual strength decreased with increasing fatigue stress (Rose 1965), while Curtu et al. (1969) also noted that fatigue damage in ash was concentrated near rays, suggesting their role in fiber bundles sliding. Larger specimens showed greater deformation, likely due to more inherent defects, especially in longitudinal loading.

## 4 Materials and methods

A series of experimental fatigue tests, followed by short-term compressive strength tests, were conducted on knot-free specimens of medium-density ash wood (*F. excelsior*). The samples were collected from boards cut at different heights of the tree and taken randomly from these boards to capture material variability. The specimens, measuring  $25 \times 25 \times 75$  mm, were cut with fibers straight and parallel to the longitudinal direction (loading direction). An 8802

Instron servohydraulic machine was used to conduct both the short-term and fatigue tests. An Advanced Video Extensometer (AVE 2) was attached to the machine to measure strain. The average strain was measured over a gauge length of 60 mm on the specimen during the test. Two different batches of specimens were used to investigate the interval effect and the frequency effect, respectively. The first batch consisted of 44 samples, while the second batch consisted of 21 samples. For each batch, a separate static test was conducted, using at least 12 specimens from that batch, to determine the reference short-term strength for the corresponding fatigue tests. The experimental setup in Figure 1 illustrates the specimen mounting and video extensometer gauge length for strain measurements.

### 4.1 Static test

The objective of the static test was to investigate the distribution of short-term compressive strength in order to determine an effective mean value for setting the stress level (SL) in subsequent fatigue tests for each batch.

For the first batch, 28 specimens were conditioned at a relative humidity of 65 % and a temperature of 20 °C. The specimen density ranged between 580 and 720 kg/m<sup>3</sup>. For the second batch with a density range between 580 and 620 kg/m<sup>3</sup>, 12 specimens were conditioned under the same conditions. The annual ring width and angle on the cross-sections were recorded before testing.

A displacement-controlled test was conducted at a speed of 0.6 mm/min, with a static break detector set to trigger at a 30 % stress drop to terminate the test. Data logging rate was set to a frequency of 4 Hz.

The short-term strength showed a clearer correlation to density than to the other parameters (ring width and angle). For the first batch, the mean density of all 28 specimens was  $645 \pm 50$  kg/m<sup>3</sup>, with a mean short-term strength of  $51.1 \pm 6.2$  MPa. To reduce variation, the density range was narrowed to 580–620 kg/m<sup>3</sup>, resulting in a mean density of  $595 \pm 10$  kg/m<sup>3</sup> for 12 specimens, with a mean strength of  $45.5 \pm 1.8$  MPa. This value was used as the reference for short-term strength for this batch in fatigue tests. For the second batch, the mean density of 12 specimens was  $600 \pm 10$  kg/m<sup>3</sup>, with a mean strength of  $53.2 \pm 3.0$  MPa, which was used as a reference value for short-term strength for this batch in fatigue tests.

### 4.2 Fatigue test

For the first batch, four groups (1A to 1D), each consisting of four specimens with densities between 580 and 620 kg/m<sup>3</sup>,

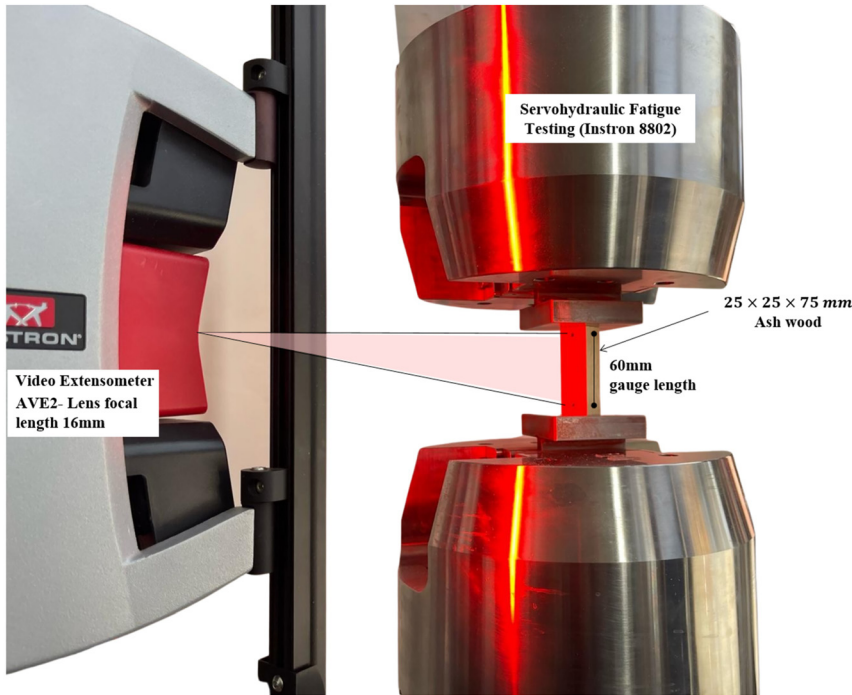


**Figure 1:** Wood specimen undergoing servohydraulic fatigue tests showing the experimental setup and specimen mounting configuration.

were selected for fatigue testing. The goal was to conduct intermittent fatigue tests to investigate the interval effect and the history effect. In this study, the 'interval effect' refers to how variations in the intermittent fatigue loading intervals influence fatigue strain development, while keeping the total number of cycles (NOC) constant. Whereas the 'history effect' describes the dependency of the material's current strain response on its previous loading history. The tests were performed at a frequency of 1 Hz, using a sinusoidal waveform with a 77.6 % stress level (35.3 MPa) and a stress ratio of  $R = 10$ . The test plans were prepared using WaveMatrix software. The loading sequence, as shown in Figure 2a, consists of two main stages: repeated loading and static loading. The repeated loading stage comprises loading loops ( $L_N$ ); each loop consists of four stages: ramp loading with a stress rate of 0.6 MPa/min to reach  $0.1 \sigma_s$ , cyclic loading ( $N_C$ ) varying between  $0.1$  and  $1 \sigma_s$ , ramp unloading within 5 s, and a recovery phase ( $T_{rev}$ ) allowing the strain to recover before the following loop.

For the second batch, three groups, each consisting of three specimens with densities between 580 and 620 kg/m<sup>3</sup>, were tested at three different frequencies: 0.1 Hz, 1.0 Hz, and 10.0 Hz. The stress value of 35.5 MPa was applied, resulting in a stress level of 66.7 %. The objective was to investigate the effect of frequency on strain accumulation, recovery, material stiffness, and residual strength. The loading sequence, as shown in Figure 2b, was similar to that of the first batch but without loading loops.

Table 1 shows the test setup and experimental condition for each group. After completing the repeated loading stage, static loading commenced at a loading speed of 0.6 mm/min. The data logging of the strain measurements during the repeated loading was set to a frequency of 10 Hz. The specimens' weight was measured immediately before and after the test to assess the loss in moisture content. An average loss of around 0.3 % was recorded across all test groups. Even for the longest test group 1.0C, the test duration was roughly 135 min. Given the relatively short test durations and minimal moisture changes, the test conditions were considered to represent a quasi-constant climate, even without active climate control. For future studies involving longer testing periods, the use of a climate chamber to control relative humidity and temperature during cyclic loading is recommended.

### 4.3 Micro CT-scan

X-ray micro-computed tomography ( $\mu$ CT) was used to obtain high-resolution 3D structures of ash wood samples in a non-destructive way. The tomography was carried out using a *v|tome|x s 240* (Phoenix/GE, Wunstorf, Germany). This  $\mu$ CT system comprises an *xs240D* direct X-ray tube capable of a maximum X-ray energy of 240 keV and a maximum power of 300 W with a water-cooled tungsten anode. The X-ray window between the vacuum inside and the air outside the tube is 500  $\mu$ m thick and made of beryllium.

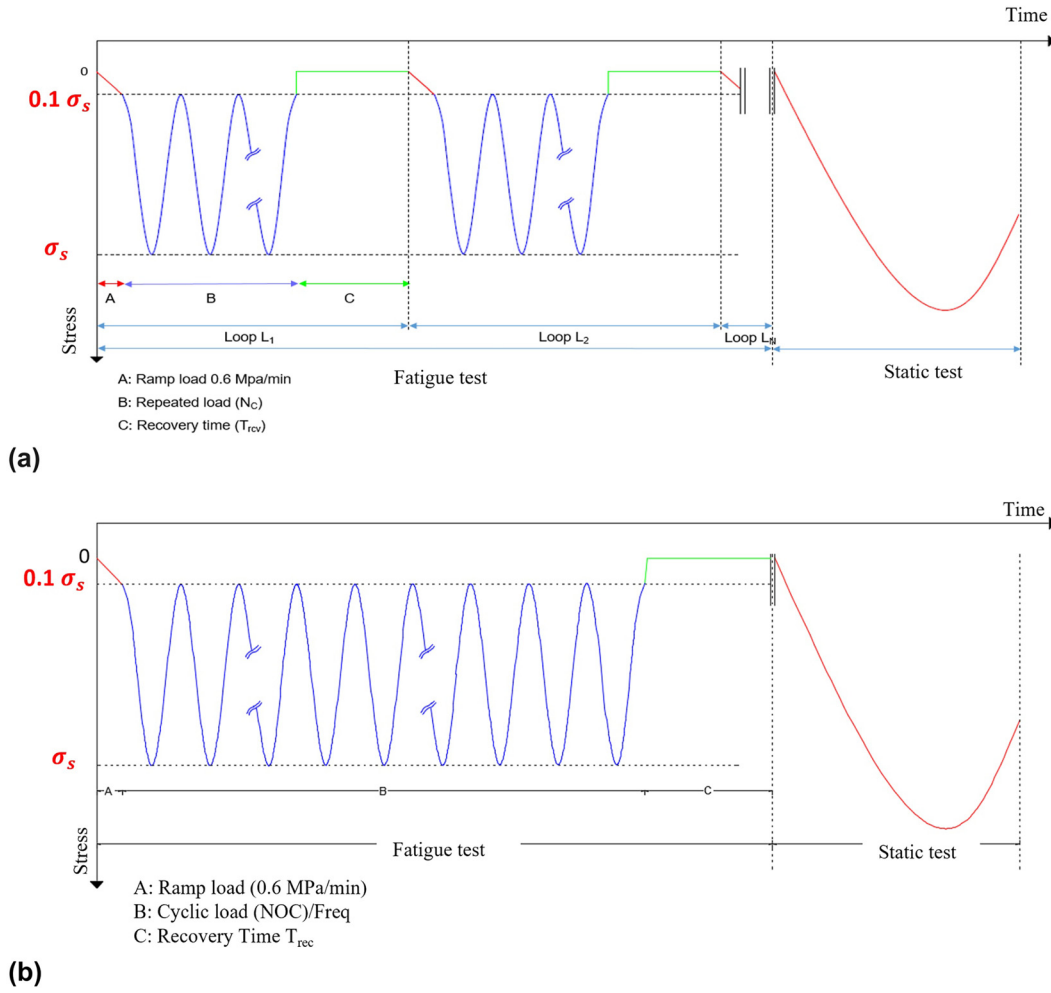


Figure 2: Loading sequences: (a) cyclic loading with recovery and loop phases, followed by static loading; (b) cyclic loading followed by static loading.

Table 1: Repeated loading: test setup and experimental plan.

Group ID	First batch				Second batch		
	1.0A	1.0B	1.0C	1.0D	0.1E	1.0F	10.0G
Frequency [Hz]	1.0	1.0	1.0	1.0	0.1	1.0	10.0
Number of cycles in each loop $N_c$	200	400	200	2,000	200	2,000	20,000
Number of loops $N_L$	5	5	10	1	1	1	1
Total number of cycles	1,000	2,000	2,000	2,000	200	2,000	20,000
Recovery time $T_{rec}$ ([s])	600	600	600	3,000	3,000	3,000	3,000
Number of samples	4	4	4	3	3	3	3
Average density [kg/m <sup>3</sup> ]	600	595	590	585	600	590	610

The flat panel type a-Si detector of the v|tome| x is a DXR250RT with 14-bit depth, directly coupled to a CsI scintillator. It has 1,000 × 1,000 pixels of 200 μm × 200 μm pitch

and is located at a fixed distance of 811.7 mm from the X-ray spot on the tungsten anode.

The geometric magnification  $M$  of the system depends on the source-to-detector distance (SDD) and the source-to-sample distance (SSD) as:

$$M = \frac{SDD}{SSD} \tag{2}$$

To increase the resolution, the v|tome| x offers a so-called virtual mode, where the detector is moved perpendicular to the rotation axis of the sample into two positions, nearly doubling the number of effective detector pixels in this direction. Twenty central columns of pixels overlap and are used to adjust the projected intensities from the two detector positions.

During the measurements, the X-ray tube operated at a peak voltage of 50 kV, using the full X-ray spectrum of the tungsten anode. No additional filters were applied beyond the beryllium window. The maximum power was limited to

5 W to ensure that the power-dependent size of the X-ray spot matched the effective voxel size of the reconstructed volumes.

The minimum source-to-sample distance (SSD) – and hence the maximum magnification  $M$  and minimum effective voxel size – was constrained by the overall size of the ash wood samples. For the first sample, the obtainable isotropic voxel size was 7.3  $\mu\text{m}$ ; for the second sample, it was 7.5  $\mu\text{m}$ .

## 5 Results and discussion

The findings of this study are structured into three subsections. First, the residual strength and stiffness are examined to assess the material's mechanical performance after fatigue loading. Second, the strain accumulation during fatigue and strain recovery is analyzed to understand the progressive deformation and recovery behavior of the specimens. Third, the frequency effect on the strain development is investigated in detail. The microstructural changes from CT-scanning are analyzed separately in a following chapter.

### 5.1 Residual strength and stiffness

The mean short-term strength observed after cyclic loading for the tested groups varied slightly. For the first batch, which was tested at a 1 Hz frequency, Groups 1.0A, 1.0B, 1.0C, and 1.0D had average strengths of 43.4 MPa, 47.1 MPa, 44.4 MPa, and 44.7 MPa, respectively. These values show only a minor reduction compared to the referenced short-term strength of 45.5 MPa, indicating that the selected number of cycles and stress level did not significantly affect the material's short-term strength. Figure 3a illustrates the stress-strain relationship from short-term compression tests after cyclic loading (first setup with cycle loops).

For the second test setup, Groups 0.1E, 1.0F, and 10.0G, which were tested at 0.1 Hz, 1.0 Hz, and 10.0 Hz, respectively, exhibited average strengths of 51.5 MPa, 50.7 MPa, and 52.9 MPa. These values also showed a minor change compared to the referenced short-term strength for this batch (53.2 MPa). The stress-strain relationships for these groups are detailed in Figure 3b, illustrating the stress-strain relationship from short-term compression tests after cyclic loading (second setup with cyclic loops). Two possibilities exist: either the residual strength is not affected by the relatively short-period fatigue testing, or the strength degradation is partially compensated by a densification effect. The densification theory aligns with Gong and Smith

(2005), who reported a 4 % increase in residual strength of black spruce following low-cycle fatigue (LCF) loading at 75 %, 85 %, and 95 % of the ultimate stress. Two possible mechanisms have been proposed to explain this increase in residual strength: 1. the strength increased due to moisture content loss because of the induced temperature during cyclic loading (Dobraszczyk 1983) or 2. densification via fiber buckling and microfibril reorientation in the cell wall (Rose 1965) – at the current experimental setup, the maximum test duration (33 min for Group 1.0D) was too brief for significant temperature-induced MC changes. Thus, densification effects likely explain the observed strength stability in these tests.

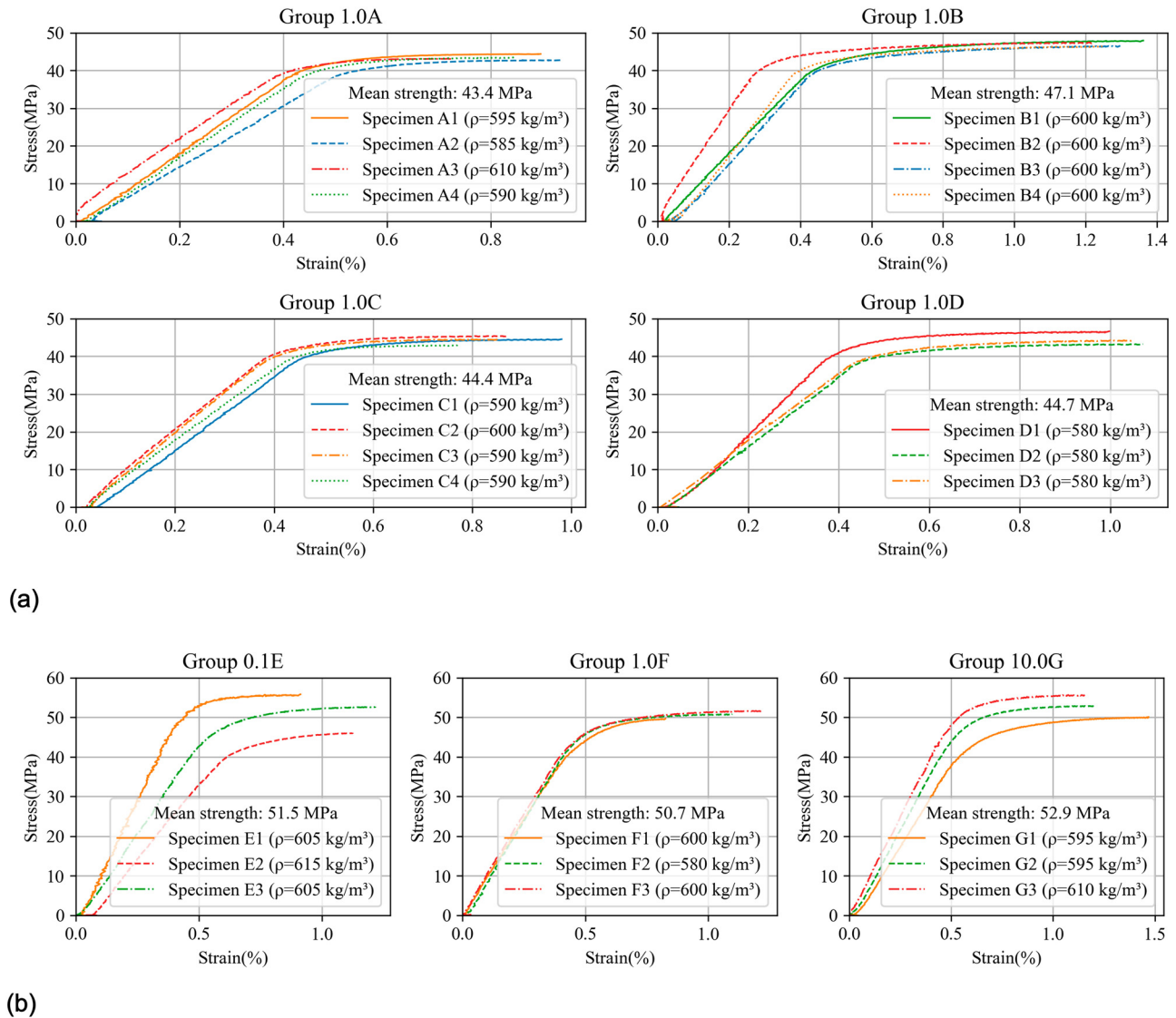
The average stiffness values for groups 1.0A, 1.0B, 1.0C, and 1.0D of the first test setup were calculated as 9.6 GPa, 12.2 GPa, 10.8 GPa, and 10.6 GPa, respectively. These values were calculated from the initial loading cycle. Meanwhile, for the second batch, values of 10.4 GPa, 10.8 GPa, and 9.8 GPa were calculated for groups 0.1E, 1.0F, and 10.0G. Monitoring cyclic stiffness during fatigue loading is a key method for evaluating material deterioration during repeated loading. The cyclic stiffness ( $E_N$ ) was calculated using Eq. (1).

Figure 4a shows the computed stiffness during cyclic loading for the first test setup. The influence of frequency on cyclic stiffness is displayed in Figure 4b, revealing no significant variation throughout the cyclic loading process.

Previous studies have reported differing observations on stiffness evolution before fatigue failure. Gong and Smith (2005) found no notable stiffness changes in spruce within 120 load cycles under low-frequency (0.2 Hz) compression fatigue at stress levels (SLs) ranging from 75 % to 95 %, which is consistent with our results. In contrast, Ogawa et al. (2017) observed more pronounced fluctuations in Japanese cypress LVL during long-term fatigue tests (up to 0.8 million cycles) under perpendicular-to-grain loading at SLs of 60–120 %. Stiffness remained stable at SLs  $\leq$  80 %, possibly due to a “strengthening” effect from densification in the radial direction, while higher SLs led to progressive reduction. Gong and Smith (2000) also documented increased stiffness reduction until failure in parallel-to-grain tests at 90 % SL. These findings suggest that for stress levels exceeding 80 % of the reference short-term strength, material stiffness is more likely to decrease in low-cycle fatigue tests compared to stress levels below 80 %.

### 5.2 Intermittent loading

The strain and strain recovery results were compared for all test groups in the first batch in order to study the effect of intermittent fatigue loading. Although the selected density



**Figure 3:** Stress–strain relationships from short-term compression tests after cyclic loading. (A) First setup with cyclic loops. (B) Second setup with different frequencies.

range helped to maintain relatively low variability in short-term strength ( $45.5 \pm 1.8 \text{ MPa}$ ), the measured strain magnitude across different specimens under the same stress differed. To facilitate meaningful groupwise comparison, a post-processing procedure was introduced, containing the following steps:

- **Normalization:** For each specimen, the cyclic strain was normalized based on its initial strain at the maximum stress of the first NOC ( $\varepsilon_0$ ).
- **Data reduction:** Since we are only interested in the evolution of maximum accumulated strain ( $\varepsilon_{acc}$ ) and strain recovery ( $\varepsilon_{re}$ ), only the bounding curve of the strain-time or strain-NOC curves was considered in the subsequent plots.

- **Mean extraction:** A mean curve was then calculated for the three to four specimens in each group for the groupwise comparison.

### 5.2.1 Specimen variation

Despite careful selection to ensure comparable properties among the tested specimens, some variation of density is still expectable. To account for these variations, the overall strain evolution for Group 1.0A and Group 1.0C, both of which underwent identical testing procedures during the first five loading loops were compared. As depicted in Figure 5,  $\varepsilon_{acc}$  and  $\varepsilon_{re}$  showed no significant deviation between the two groups.

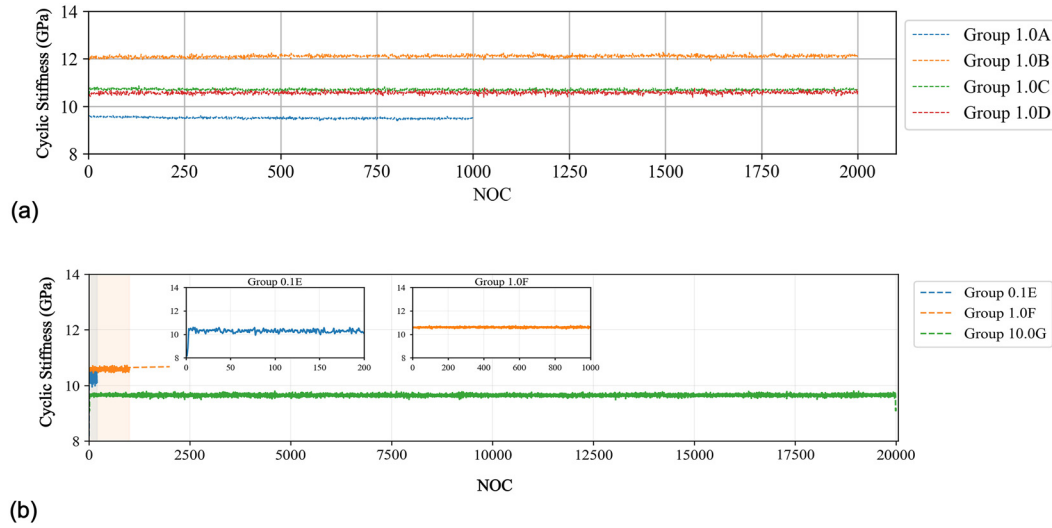


Figure 4: Stiffness during cyclic loading: (a) first batch with cyclic loops; (b) second batch with different frequencies.

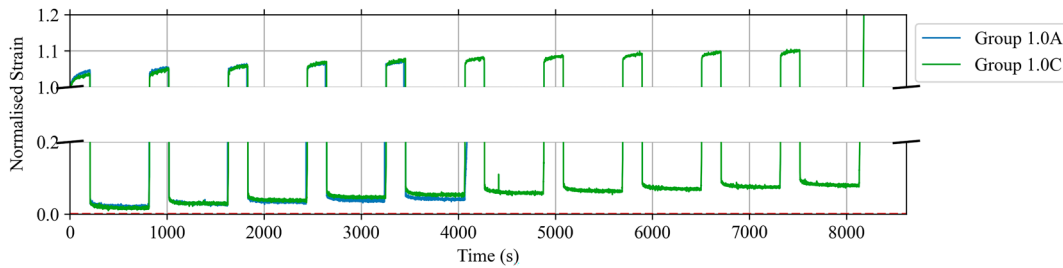


Figure 5: Comparison of accumulated strain  $\epsilon_{acc}$  and residual strain  $\epsilon_{re}$  for Group 1.0A and Group 1.0C (plotted over time).

### 5.2.2 Interval effect

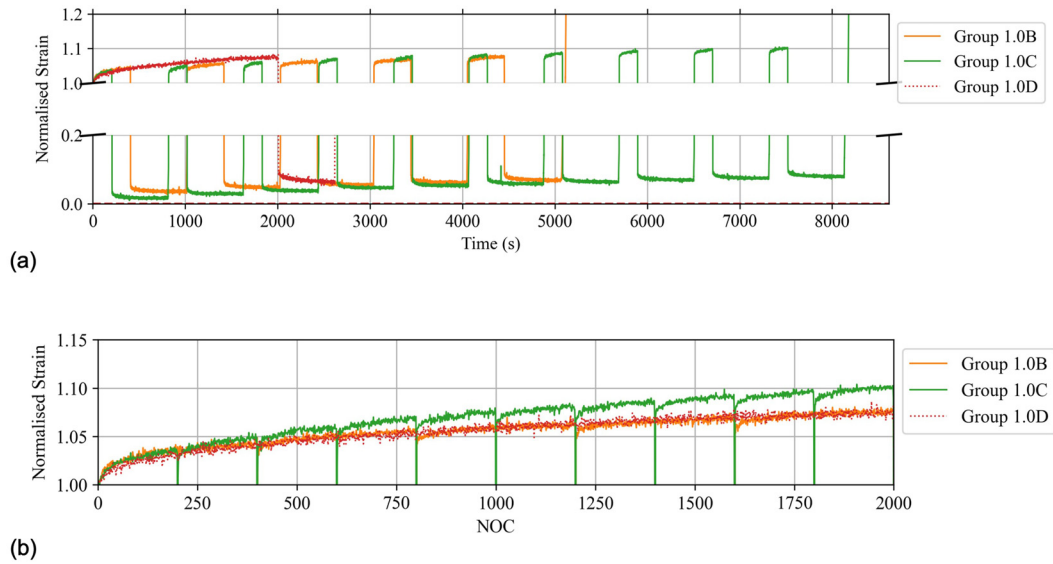
Three groups from the 1 Hz tests were compared to investigate the effect of the loading interval: Group 1.0B, Group 1.0C, and Group 1.0D. All three groups were designed to have the same total number of cycles (NOC = 2,000). However, the loading was divided into 5 and 10 equal loading loops for Group 1.0B and Group 1.0C, respectively, while specimens in Group 1.0D were subjected to continuous fatigue loading of 2,000 cycles.

Figure 6a provides a comparison of both  $\epsilon_{acc}$  and  $\epsilon_{re}$  plotted over time. It can be observed that, all the fatigue loading and recovery curves showed an asymptotic trajectory, similar to creep curves. For  $\epsilon_{acc}$ , the comparison can be clearly seen in Figure 6b, where the normalized strain is plotted over NOC. All groups exhibited similar strain evolution trend. There appeared to be no significant interval effect within the NOC span of interest when comparing Group 1.0B and Group 1.0D. Although the group with shorter

loading period exhibited lower strain after each recovery phase, this difference was quickly offset by its higher strain increase rate at the beginning of the subsequent loading. For Group 1.0C, the first two loading loops revealed similar trend. However, starting from the third loading loop, Group 1.0C exhibited higher rate of strain accumulation, leading to a total  $\epsilon_{acc}$  increase that was approximately 30 % higher than of the other groups at the end of 2,000 cycles. Moreover, the recovery curves for Group 1.0B and Group 1.0D showed similar magnitude after 2,000 cycles, despite the different loading intervals and different total recovery time. For Group 1.0C, which showed higher  $\epsilon_{acc}$ , the residual strain at the end also appeared to be slightly higher than the other groups.

### 5.2.3 History effect

The strain accumulation during each loading loop within the same test group was analyzed in detail to investigate the



**Figure 6:** Comparison of accumulated and residual strain for Group 1.0B, 1.0C and 1.0D: (a) plotted over time; (b) plotted over number of cycles (NOC).

potential history effect. Figure 7 illustrates the comparison of strain accumulation across loading loops, with the origin of time set at the beginning of each loading loop. Groups 1.0A, 1.0B and 1.0C were compared, as these groups contained multiple loading loops. The hypothesis was that if there is no history effect, the slope of the first loading loop should be identical to that of all subsequent loading loops within the same test group. From the data, a steady increase in strain was observed across all loading loops, characterized by rapid accumulation at the beginning of each loop and a gradual slowdown in subsequent loops. Notably, the strain accumulation trend from the second loop onward exhibited a nearly parallel trajectory. In contrast, the first loop demonstrated a significantly higher initial strain accumulation rate compared to the others. Figure 8 visualises this difference by quantifying the net increase of normalised strain within each loading loop. It can be observed that the highest net strain increase occurred during the first loading loop for the compared test groups.

Similar comparison was performed for the strain recovery. In this work, the recovery period was set to an equal duration of 600 s for Groups 1.0A, 1.0B and 1.0C. According to Figure 9, the selected recovery duration seemed to be sufficient to recover all the viscoelastic strain component, as the recovery curves gradually leveled off into an asymptotic horizontal line by the end of the recovery period. Unlike the  $\varepsilon_{acc}$ , all loading loops show a nearly parallel trajectory, suggesting no history effect on the strain recovery.

### 5.3 Frequency effect

Understanding the effect of loading frequency on fatigue strain accumulation is complex due to multiple interacting factors, the most dominant of which being the time-dependent mechanism (duration of the total fatigue loading), cycle-dependent mechanism (NOC) and the rate-dependent mechanism (the loading rate at which fatigue cycles are applied). Specifically, if the applied stress is kept the same, at a given NOC, groups with higher frequency undergo a shorter load duration and a higher loading rate, both of which are anticipated to contribute to a lower strain accumulation. When comparing the same loading period, however, the effect of higher loading rate might be partially or completely offset by the greater number of cycles for higher frequencies. To test the above-mentioned hypothesis and further explore the interaction among different factors,  $\varepsilon_{acc}$  was compared across different groups – 0.1E, 1.0F and 10.0G, plotted over both NOC and time.

Figures 10 and 11 illustrate the comparison plotted over time and over NOC, respectively. From both graphs, it can be observed that  $\varepsilon_{acc}$  of the higher frequency groups was consistently lower than that of the lower frequency groups. Furthermore, the difference of accumulated strain between 10 Hz and 1 Hz appeared to be lower than that between 1 Hz and 0.1 Hz. However, the strain recovery,  $\varepsilon_{re}$  for the 10 Hz group could not be distinguished from that of the 1 Hz group. Nevertheless, both groups were featured by a much lower

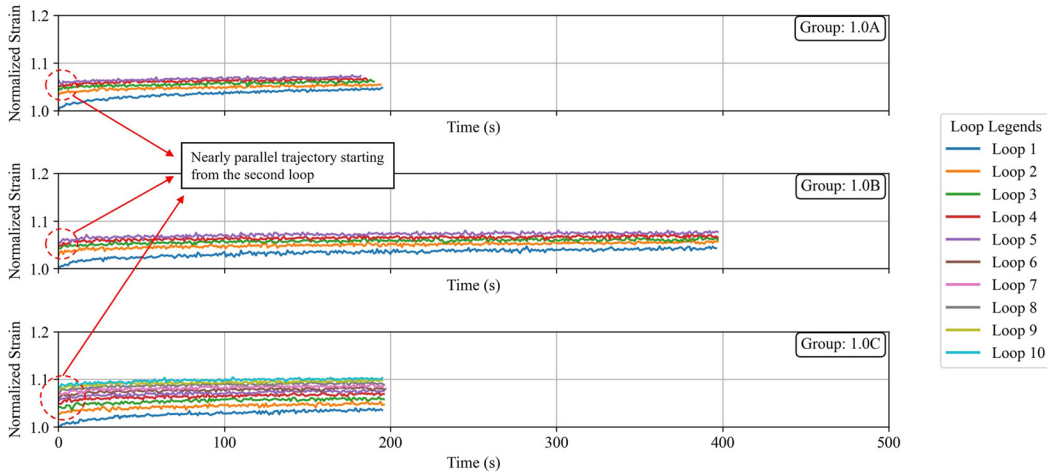


Figure 7: Comparison of accumulated strain  $\epsilon_{acc}$  for each loop in Group 1.0A, 1.0B and 1.0C (plotted over time).

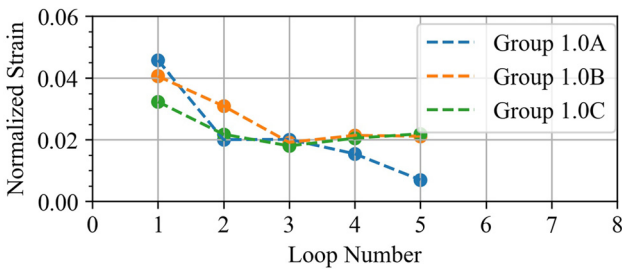


Figure 8: Comparison of accumulated strain  $\epsilon_{acc}$  for each loop in Group 1.0B, 1.0C and 1.0D (plotted over loading loop).

magnitude of strain during the entire recovery period compared to the 0.1 Hz group.

This observation is inline with the previous findings in Okuyama et al. (1984), Clorius et al. (2000) and Sasaki et al. (2014), where compressive, compressive and bending fatigue with different frequencies were compared, respectively. Except for the group tested under lower relative humidity or with frequencies lower than 1 Hz in Clorius et al. (2000), the above-mentioned literature all suggested a prolonged fatigue life under higher loading frequencies. Therefore, there is potential to use the normalised accumulated strain as a

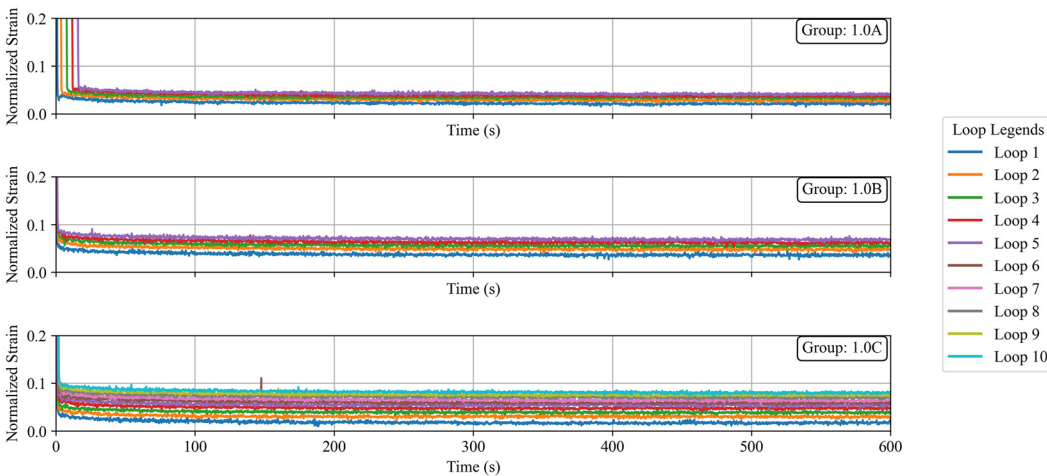
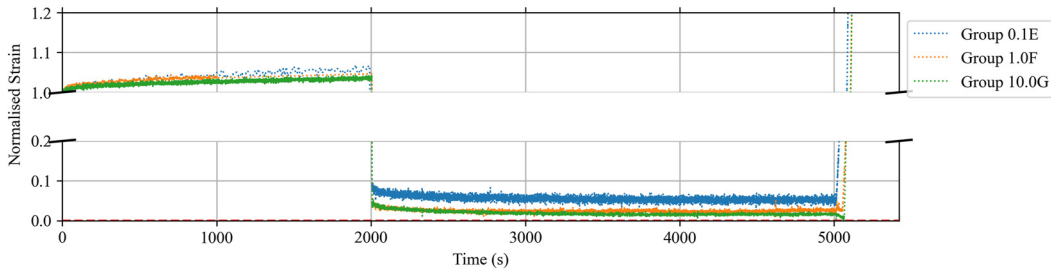
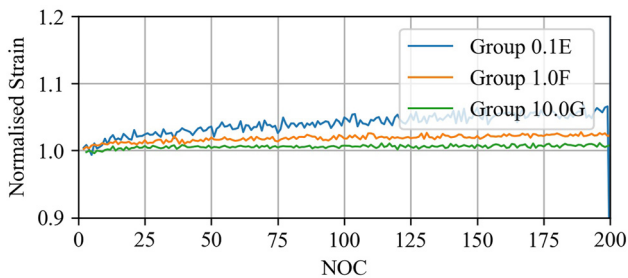


Figure 9: Comparison of residual strain  $\epsilon_{re}$  for each loop in Group 1.0A, 1.0B and 1.0C (plotted over time).



**Figure 10:** Comparison of accumulated strain  $\varepsilon_{acc}$  and residual strain  $\varepsilon_{re}$  for Group 0.1E, 1.0F and 10.0G (plotted over time).



**Figure 11:** Comparison of accumulated strain  $\varepsilon_{acc}$  for Group 0.1E, 1.0F and 10.0G (on NOC scale).

physical indicator for “damage” in fatigue, where higher relative increase in  $\varepsilon_{acc}$  can be correlated to shorter fatigue lives.

## 6 Microstructural damage

As explained in the methodology part, high-resolution  $\mu$ CT was employed to investigate internal damage mechanisms associated with compression fatigue in wood and visualize the development of microcracks. To reconstruct the  $\mu$ CT results accurately, 3,201 projections of 3 s each were recorded and reconstructed with standard filtered back projection, FBP, using the software *X-AID* (Version 2024.4.0, Mitos GmbH, Munich, Germany). After each rotation step, a projection of 1 s was neglected to reduce the influence of an afterglow of the CsI scintillator material of the detector. Hence, a tomography took about 3.5 h. After an optimization of parameters for reconstruction, a FBP took about 20 s on a 64 bit, 16 core, 1.5 GHz computer with sufficient memory. This non-destructive technique, although time consuming, compared to the standard scanning methods, enabled internal inspection of structural changes in a micro level, while preserving specimen integrity, making it well-suited for assessing fatigue-induced damage.

A specimen from group (1.0 D) subjected to cyclic compression fatigue at 1 Hz and 75 % stress level (SL),

followed by a short-term static loading phase, exhibited distinct microstructural damage. As illustrated in Figure 12a (where the obtainable isotropic voxel size after  $\mu$ CT was 7.3  $\mu$ m),  $\mu$ CT results show a dominant kink band along with several secondary kink bands near the main fracture surface. These secondary features suggest subcritical damage accumulation resulting from repeated loading. In comparison, the reference specimen loaded under monotonic compression (Figure 12b) (where the obtainable isotropic voxel size after  $\mu$ CT was 7.5  $\mu$ m) displayed a single, sharply defined primary kink band with no visible secondary damage – indicating a more localized and brittle failure. These results are more visible in the reconstructed 3D image of the scanned area, as illustrated in Figure 13. These observations are consistent with prior findings by Bonfield and Ansell (1991), who reported diffuse fatigue damage in Douglas fir, and Gong and Smith (2000), who observed progressive microstructural damage in spruce under compression fatigue, including the formation of pre-kinks, full kinks, and creases in tracheid cell walls, ultimately leading to macroscopic shear bands through microfibril buckling.

The results highlight that fatigue loading leads to more internal microstructural damage compared to static loading, even when failure occurs at similar stress levels. Scanning technologies help to visualize such mechanisms and to identify early damage features that are not detectable through conventional mechanical testing.

## 7 Conclusions

This study investigated the compressive fatigue behavior of European ash wood through a combination of mechanical testing and high-resolution microstructural scanning techniques. The findings offer valuable insights into strain accumulation, residual mechanical properties, time- and rate-dependent deformation, and internal damage evolution under cyclic loading.

Residual strength and stiffness were only slightly affected by fatigue loading. This suggests a potential

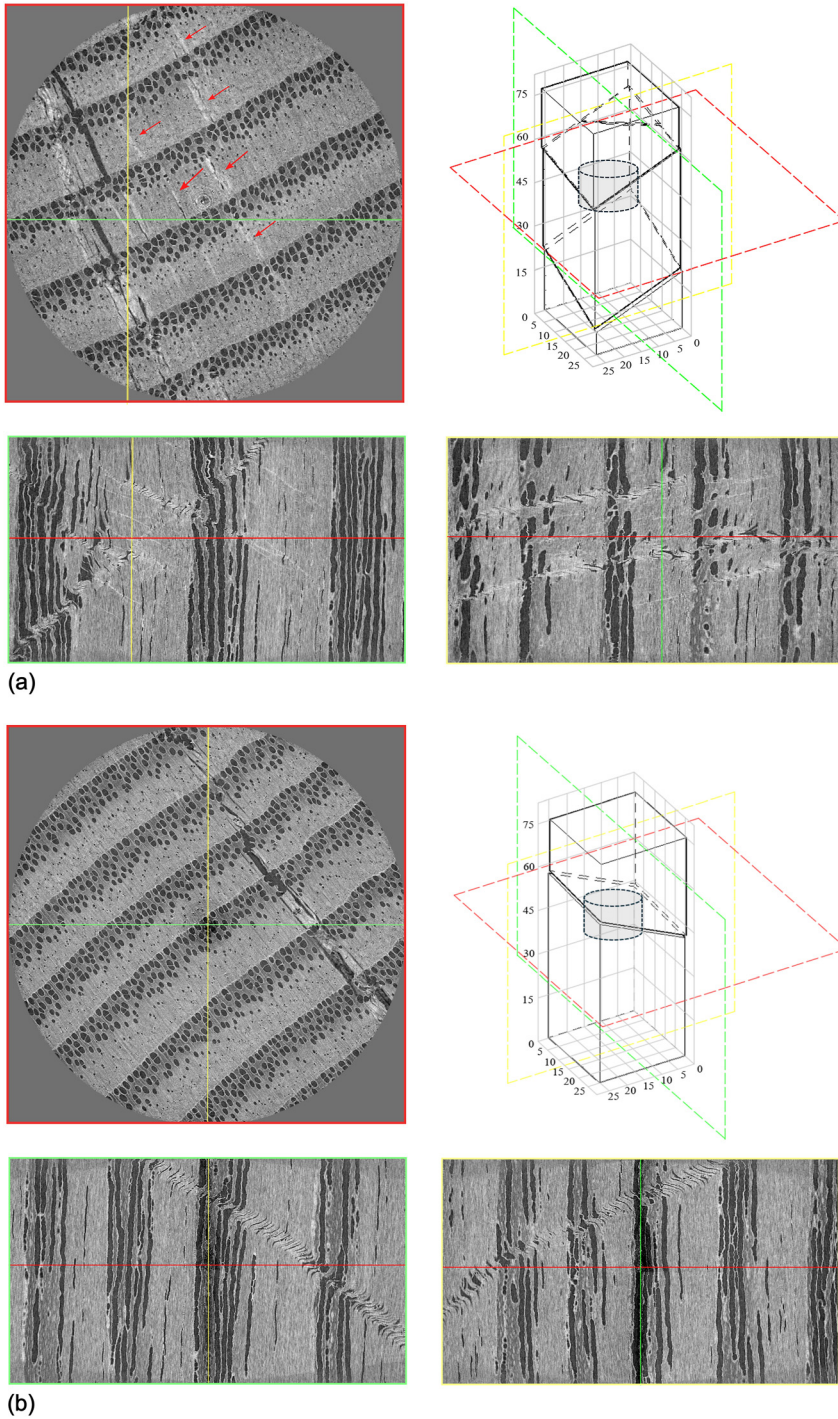


**Figure 12:** CT scan with voxel size of  $7.3 \times 7.3 \times 7.3 \mu\text{m}$ : (a) compression fatigue at 1 Hz, 75 % SL, followed by a short-term test showing minor kink bands beside the main kink band; (b) short-term compression test at 0.6 mm/min displacement rate showing the main kink band.

densification effect through fiber buckling or microfibril reorientation. Intermittent loading tests confirmed the presence of both viscous and viscoelastic components. The viscoelastic component (recovery curve) remained consistent despite different intermittent loading histories. However, history effect was observed in total accumulated strain (particularly in the first loading loop). Given the same loading duration, higher frequencies led to lower

overall strain accumulation. However, recovery strains at high frequencies were not significantly different from those at moderate frequencies, highlighting the complex interaction between time-, cycle-, and rate-dependent damage mechanisms. However, Micro-CT imaging revealed the development of diffuse microcracks under fatigue loading, which were less apparent under static loading, which affirms that even low-cycle fatigue can

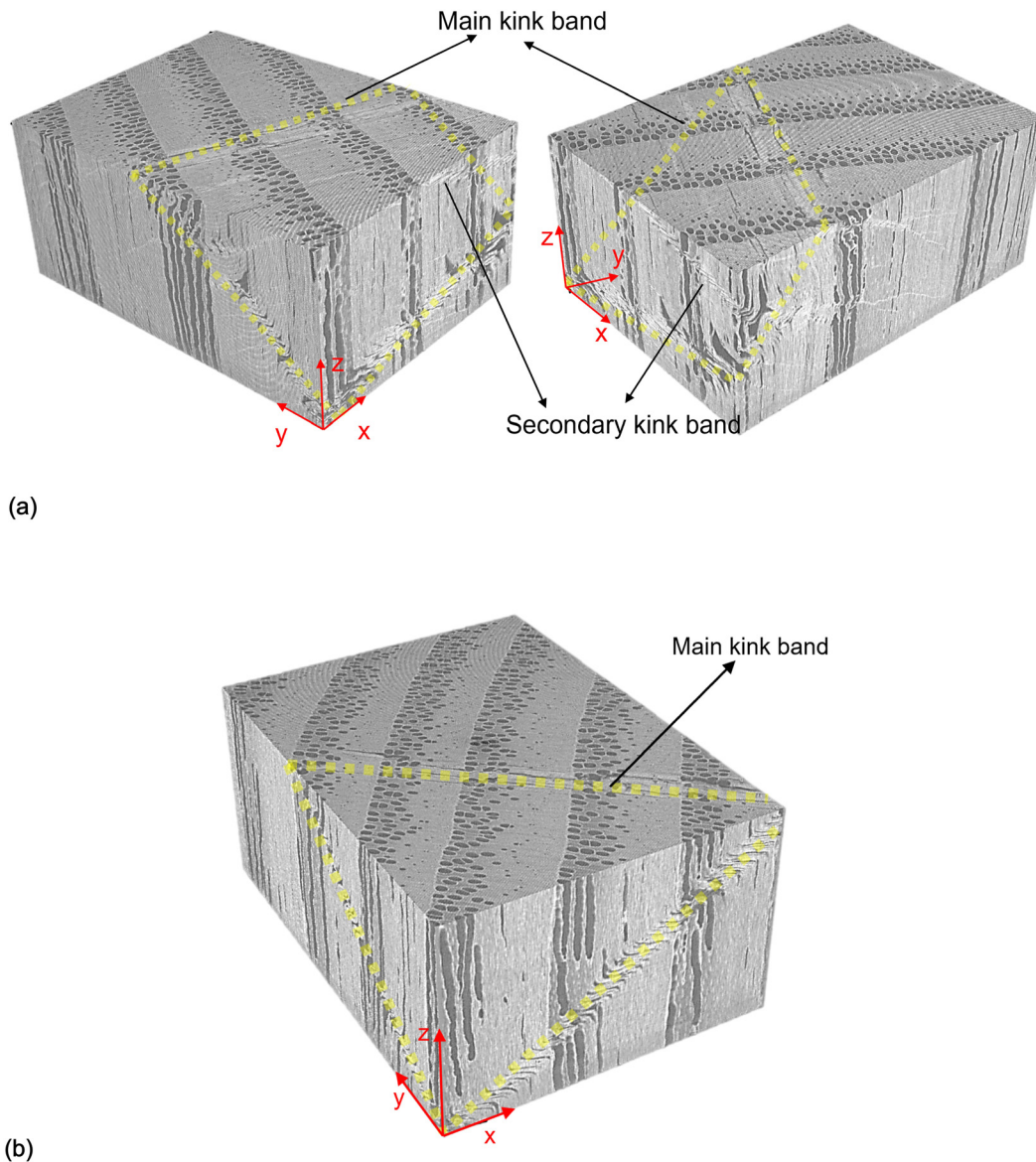


**Figure 13:** 3D reconstruction of the CT-scan: (a) 3D reconstruction of the CT-scan results for the fatigued sample; (b) 3D reconstruction of the CT-scan results for the short-term tested sample.

trigger subcritical microstructural degradation, invisible to conventional mechanical testing.

**Acknowledgements:** The authors gratefully acknowledge the Bavarian State Ministry of Food, Agriculture, and Forestry for funding the WoodVibes project and for providing climate-controlled fatigue testing equipment.

**Research ethics:** Not applicable.

**Informed consent:** Not applicable.

**Author contributions:** M. Abdelrahman and C. Yang designed, performed the experiments, analyzed the outcomes, and wrote the manuscript. K. Achterhold and F. Pfeiffer performed the CT scanning. A. Khaloian and J.W. Van de Kuilen supervised the lab work, reviewed, and edited the manuscript.

All authors have accepted responsibility for the entire content of this manuscript and approved its submission.

**Use of Large Language Models, AI and Machine Learning Tools:** None declared.

**Conflict of interest:** The authors state no conflict of interest.

**Research funding:** This work was supported through two funding sources: (1) the German Federal Ministry of Food and Agriculture, administered by the Fachagentur Nachwachsende Rohstoffe e.V. (FNR) [Grant No. 22009817, HS-Hybrid project], and (2) the Bavarian State Ministry of Food, Agriculture and Forestry [Grant ID: LWF-A9-7831-26-4-1, WoodVibes project].

**Data availability:** Not applicable.

## Appendix: Literature summary table

**Table A1:** Experimental studies on wood under uniaxial fatigue loading.

Literature	Loading type (direction to the grain)	Wood species	NOC	Frequency (Hz)	SL %	Waveform	R-ratio	T (°C)	RH/MC
Kellogg (1960)	Tension (parallel)	Solid wood: Dietrich Cofrio, Känsefäret Timbasika, Hickory Manni (Chewstock) – CRiba, Redwood, White pine	100	0.001– 0.0005	0	–	–	32	9–13 % MC
Möhler and Ehlbeck (1968)	Four-point bending	Particleboard from pine	75	/1 week,/ 1 month	40–90	–	0.5	–	9.4– 11.4 % MC
Curtu et al. (1969)	Compression (parallel)	Solid wood: Ash	8	8 min	8.8 (para) 1.3 (perp)	Square	–	20	12 % MC, 65 % RH
Bach (1975)	Compression (parallel)	Solid wood: Pine	0.1	0.01, 0.0001	0	Square	–	20	15 % MC, 75 % RH
Okuyama and Mar- soem (1987)	Tension (parallel)	Solid wood: Silka spruce	400	1	30–90	Sinusoidal, square	0	20	12 % MC
Tokuda (1987)	Shear test	Plywood and Particleboard: Shear wall panel (ham-fri)	2,000	0.003	30–80	–	–1	–	12– 15 % MC
Clorius et al. (2000)	Compression (parallel)	Solid wood: Spruce	100–10	0.01; 1; 10	80	Square	–	25	65 % RH
Gong and Smith (2000)	Compression (parallel)	Solid wood: Dark spruce	120	0.5	90	Square	–	25	85 % RH
Gong and Smith (2005)	Compression (parallel)	Solid wood: Dark spruce	120	0.5	20–40, 60, 80	Sinusoidal	–	20	14.5 % MC
Gong (2002)	Compression (parallel)	Solid wood: Dark spruce	120	0.2	73, 85, 95	Triangular	–	20	75 % RH
Kent et al. (2005)	Tension & compression (parallel)	Solid wood: Douglas fir lumber	0.08	–	38, 23, 30	–	0.2	20	12 % MC
Chen et al. (2006)	Tension (parallel and perpendicular to 0, 45, 90 deg angle)	Solid wood: Red Launa, Silka spruce	70–350	0.17	90, 80, 70, 50, 30	Triangular	Unidirectional load	–	–
Li et al. (2012)	Tension & compression (parallel)	Solid wood: white ash and Hickory	25	0.5	85	Sinusoidal	–	20	65 % RH, 12 % MC
Li and Lam (2016)	Shear test	CLT	281,212	–	–	Trapezoidal	–	–	–
Carvalho et al. (2022)	Three-point bending	Solid wood: Chietta	4,500	0.5, 1	–	–	–	–	–
Yang et al. (2025)	Compression (parallel)	Solid wood: Ash	2,000, 10e5	1	78	Sinusoidal	0.1	20	65 % RH

## References

- Armstrong, L.D. and Christensen, G.N. (1961). Influence of moisture changes on deformation of wood under stress. *Nature* 191: 869–870.
- Bach, L. (1973). Reiner-Weissenberg's theory applied to time-dependent fracture of wood subjected to various modes of mechanical loading. *Wood Sci.* 5: 161–171.
- Bach, L. (1975). Prepared at MacMillan Bloedel Research, Vancouver, B.C., Canada. Presented at the Forest Products Research Society Annual Meeting, Portland, Oregon, U.S.A., 15 June 1975.
- Bond, I. and Ansell, M.P. (1998). Fatigue properties of jointed wood composites – part I statistical analysis, fatigue master curves and constant life diagrams. *J. Mater. Sci.* 33: 2751–2762.
- Bonfield, P.W. and Ansell, M.P. (1991). Fatigue properties of wood in tension, compression and shear. *J. Mater. Sci.* 26: 4765–4773.
- Carvalho, J.S., Christoforo, A.L., Lahr, F.A.R., and Aquino, V.B.D.M. (2022). Effect of fatigue on tropical wood species. *Ambiente Construído* 22: 187–198.
- Chen, Z., Gabbitas, B., and Hunt, D. (2006). The fracture of wood under torsional loading. *J. Mater. Sci.* 41: 7247–7259.
- Clorius, C.O. (2002). *Fatigue in wood: an investigation in tension perpendicular to the grain*, PhD thesis. Kgs. Lyngby, Denmark, Technical University of Denmark.
- Clorius, C.O., Pedersen, M.U., Hoffmeyer, P., and Damkilde, L. (2000). Compressive fatigue in wood. *Wood Sci. Technol.* 34: 21–37.
- Curtu, I., Paraschiv, N., and Fleischer, H. (1969). Die Verformung druckbeanspruchten Eschenholzes in Abhängigkeit von der Probengröße. *Holz als Roh- und Werkstoff* 27: 49–54.
- Dobraszczyk, B. (1983). *An investigation into the fracture and fatigue behaviour of wood*, PhD thesis. Bath, UK, University of Bath.
- Gillwald, V.W. (1961). Beitrag zur Bestimmung der Formänderung von Holz unter schwingender Beanspruchung. *Holz als Roh- und Werkstoff* 19: 86–92.
- Gong, M. (2002). *Failure of spruce under compressive low-cycle fatigue loading parallel to grain*, PhD thesis. Canada, The University of New Brunswick.
- Gong, M. and Smith, I. (2000). *Failure mechanism of softwood under low-cycle fatigue load in compression parallel to grain*. Natural Sciences and Engineering Research Council of Canada, Ottawa, ON, Canada.
- Gong, M. and Smith, I. (2004). Effect of load type on failure mechanisms of spruce in compression parallel to grain. *Wood Sci. Technol.* 37: 435–445.
- Gong, M. and Smith, I. (2005). Effect of stress levels on compressive low-cycle fatigue behaviour of softwood. *Holzforschung* 59: 662–668.
- Hacker, C.L. (1995). *Fatigue damage in wood composites*, PhD thesis. University of Bath.
- Karr, U., Fitzka, M., Schönbauer, B.M., Krenke, T., Müller, U., and Mayer, H. (2022). Fatigue testing of wood up to one billion load cycles. *Holzforschung* 76: 977–984.
- Kellogg, R. (1960). Effect of repeated loading on tensile properties of wood. *For. Prod. J.* 10: 586–594.
- Kent, S.M., Leichti, R.J., Rosowsky, D.V., and Morrell, J.J. (2005). Effects of decay on the cyclic properties of nailed connections. *J. Mater. Civ. Eng.* 17: 579–585.
- Lewis, W.C. (1962). Fatigue resistance of quarter-scale bridge stringers in flexure and shear, Technical report, Forest Products Laboratory.
- Li, L., Gong, M., Smith, I., and Li, D. (2012). Exploratory study on fatigue behaviour of laterally loaded, nailed timber joints, based on a dissipated energy criterion. *Holzforschung* 66: 863–869.
- Li, Y. and Lam, F. (2016). Low cycle fatigue tests and damage accumulation models on the rolling shear strength of cross-laminated timber. *J. Wood Sci.* 62: 251–262.
- Möhler, K. and Ehlbeck, J. (1968). Versuche über das Dauerstandverhalten von Spanplatten und Furnierplatten bei Biegebeanspruchung. *Holz als Roh- und Werkstoff* 26: 118–124.
- Ogawa, K., Shimizu, K., Yamasaki, M., and Sasaki, Y. (2017). Fatigue behavior of Japanese cypress (*Chamaecyparis obtusa*) under repeated compression loading tests perpendicular to the grain. *Holzforschung* 71: 499–504.
- Okuyama, T., Itoh, A., and Marsoem, S.N. (1984). Mechanical responses of wood to repeated loading I: tensile and compressive fatigue fractures. *J. Jpn. Wood Res. Soc.* 30: 791–798.
- Okuyama, T. and Marsoem, S.N. (1987). Mechanical responses of wood to repeated loading IV: temperature-rises due to energy loss. *J. Jpn. Wood Res. Soc.* 33: 844–850.
- Rose, G. (1965). Das mechanische Verhalten des Kiefernholzes bei dynamischer Dauerbeanspruchung in Abhängigkeit von Belastungsart, Belastungsgröße, Feuchtigkeit und Temperatur. *Holz als Roh- und Werkstoff* 23: 271–284.
- Sasaki, Y., Oya, A., and Yamasaki, M. (2014). Energetic investigation of the fatigue of wood. *Holzforschung* 68: 843–848.
- Schönbauer, B., Killinger, M., Karr, U., Fitzka, M., Müller, U., Teischinger, A., and Mayer, H. (2022). Fatigue properties of wood at different load ratios tested at 50 Hz and 20 kHz. *Materialwissenschaft und Werkstofftechnik* 53: 344–354.
- Tokuda, M. (1987). Prediction of the number of cycles to failure of nailed shear-wall panels under reversed cyclic loading. *J. Jpn. Wood Res. Soc.* 33: 558–563.
- Tsai, K.T. and Ansell, M.P. (1990). The fatigue properties of wood in flexure. *J. Mater. Sci.* 25: 865–878.
- Watanabe, A., Sasaki, Y., and Yamasaki, M. (2014). Bending fatigue of wood; strain energy-based failure criterion and fatigue life prediction. *Wood Fiber Sci.* 46.
- Yang, C., Abdelrahman, M., Khaloian-Sarnaghi, A., and Van De Kuilen, J.-W. (2025). A comprehensive analysis of fatigue in wood and wood products. *Int. J. Fatig.* 194: 108807.